

# Beyond the instanton gas approach: dominant thimbles approximation for the Hubbard model

Maksim Ulybyshev<sup>1,\*</sup> and Fakher F. Assaad<sup>1,2,†</sup>

<sup>1</sup>*Institut für Theoretische Physik und Astrophysik,  
Universität Würzburg, 97074 Würzburg, Germany*

<sup>2</sup>*Würzburg-Dresden Cluster of Excellence ct.qmat, Am Hubland, 97074 Würzburg, Germany*

To each complex saddle point of an action, one can attach a Lefschetz thimble on which the imaginary part of the action is constant. Cauchy theorem states that summation over a set of thimbles produces the exact result. This reorganization of the path integral, is an appealing starting point for various approximations: In the realm of auxiliary quantum Monte Carlo methods it provides a framework to alleviate the negative sign problem. Here, we suggest to constrain the integration to the *dominant* thimbles: the thimbles attached to the saddle points with the largest statistical weight. For the Hubbard model, in a formulation where the the Hubbard Stratonovitch field couples to the charge, this provides a *symmetry* consistent approximation to the physics of the Hubbard model: constraining the integration domain does not explicitly break a symmetry. We can test this approach for the Hubbard model at half-filling on a bipartite lattice. The paper builds on the previously developed instanton gas approach, where an exhaustive saddle point approximation was constructed. We present results, showing that the dominant thimbles approximation provides results that are in remarkable agreement with the exact results for various fermionic observables including spin and charge order parameters and single electron spectral functions. We discuss implications of our results for simulations away of half filling.

PACS numbers: 11.15.Ha, 02.70.Ss, 71.10.Fd

Keywords: Hubbard model, instantons, Lefschetz thimbles

## I. INTRODUCTION

Quantum Monte Carlo (QMC) methods for frustrated spin systems or for models of correlated electrons generically suffer from the so called negative sign problem [1]. Here, stochastically sampled configurations carry a sign such that destructive interference results in a total average sign that vanishes exponentially with system size and inverse temperature. Owing to the central limit theorem, the uncertainty in the measurement scales as the inverse square root of the computational resources. For bounded computational resources this leads to fluctuations that quickly run out of control. This cancellation is formulation dependent and considerable research has been carried out so as to alleviate this problem [2, 3]. In fact, optimal formulations have the potential of reaching energy scales and system sizes that can impact understanding of non-trivial experimental relevant phenomena [4, 5].

In the realm of the auxiliary field quantum Monte Carlo approach, a possible route to alleviate the negative sign problem is the so called Lefschetz thimbles approach [6–8]. Let  $\mathbb{R}^N$  be the integration domain of the fields  $\Phi$  and  $S$  the action such that the partition function reads:

$$Z = \int d\Phi e^{-S(\Phi)}. \quad (1)$$

Cauchy theorem allows the deformation of the integration

contour without changing the final value of the integral. Let us hence complexify the fields  $\Phi$  and search for the saddle point of the complexified action. To each saddle point, one can attach a manifold in  $\mathbb{R}^N$  that is coined a Lefschetz thimble. Importantly, on the Lefschetz thimble, the imaginary part of the action is constant such that configurations belonging to the same thimble do not cancel out providing the fluctuations of complex measure are not too severe. However, since one has to sum over many thimbles, it may very well be that the contributions of different thimbles cancel out such that ultimately no progress is achieved.

The question we pose in this article is if this cancellation does not occur for non-trivial cases. In fact we wish to inquire if constraining the integration over a set of *dominant* thimbles with fixed  $\text{Im } S$  is an accurate enough approximation to the full path integral. Generically, this is a daunting task: we have to find the dominant saddle points, constrain the integration over the corresponding dominant thimbles and have benchmark results at hand, so as to gauge the quality of the approximation.

This program can be achieved for the special case of the Hubbard model at half-filling on a bipartite lattice. Particle-hole symmetry allows us to formulate a negative sign free algorithm such that numerically exact results on finite lattices are at hand in polynomial time.

Due to the absence of the negative sign problem thimbles are confined to the real domain, and are separated by the zeros of the fermion determinant, or equivalently by logarithmic divergences in the action. In fact, the weight of the configuration is proportional to the square of a fermion determinant, that by symmetry turns out to

\* maksim.ulybyshev@uni-wuerzburg.de

† fakher.assaad@uni-wuerzburg.de

be real. It is worth noting that the sign of a single determinant fluctuates very strongly such that a full Monte Carlo simulation will sample many thimbles. In previous papers [9, 10] we could describe the general structure of the saddle points for the Hubbard model depending on the employed Hubbard-Stratonovich transformation. The structure is particularly simple, when the auxiliary field couples to the charge density operator. In this case the saddle points can be easily described by the so called instanton gas model [10], which gives us an accurate prediction of the dominant saddles: the one, where the corresponding thimbles contributes at most to the partition function. Based on this, we wrote an exhaustive saddle point approximation for the Hubbard model at half filling. This model accounted for local moment formation and demonstrated remarkable agreement with unbiased QMC simulations in the structure of the high energy part of the spectrum of the single particle excitations. However, the pure saddle point approximation did not provide a correct spectrum in the vicinity of the Fermi level: it missed the appearance of the mass gap and the formation of the Mott insulator.

Here we go one step beyond the saddle point approximation. Using QMC techniques confined within a set of designated thimbles, and the previous predictions concerning the structure of the saddle points for the Hubbard model, we show that integration over the dominant thimbles accounts completely for the physics of the Hubbard model at least at half-filling: spectral functions and order parameters are next to indistinguishable from the exact results.

At present, we are able to confirm the validity of this approximation only at half filling, when we avoid the difficulties of sampling the fields over the thimble in complex space, corresponding to integration over a complicated curved manifold. There are however, strong indications that the structure of the thimble decomposition for the Hubbard model remains the same away of half filling provided that the auxiliary field couples to the charge [9]. This differs from previous papers where a single-thimble approximation is considered in the realm of a decomposition where the auxiliary field couples to the magnetization [11]. This suggests that the dominant thimbles approximation may also be a good approximation away from half-filling. In this case it will substantially alleviate the sign problem, since the phase of the action is constant by construction, and only the fluctuations of the complex measure appearing due to integration over curved manifold in complex plane contribute to the sign problem. It was shown however, that the sign problem arising from the fluctuation of the measure is substantially weaker than the one arising from the phase of the action [9, 12]. Hence we can conjecture that QMC on the dominant thimbles can boost our ability to simulate the Hubbard model away of half filling at lower temperatures and on larger lattice sizes than present methods.

The paper is organized as follows. In Sec. II we give a brief summary of Lefschetz thimbles and of the instanton

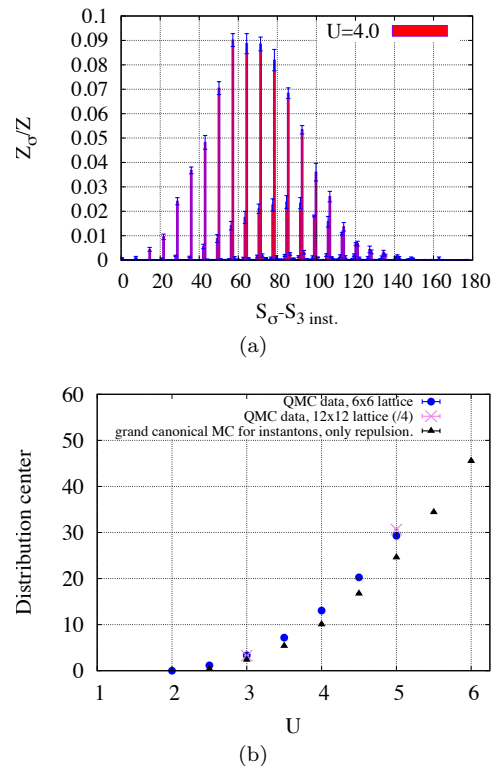


FIG. 1. (a) Histogram showing the distribution of the actions of the QMC configurations after the downwards gradient flow. The flow is long enough for the stabilization of the field configurations at the saddle points. The discrete distribution that results in *quantized* values of the action  $S$  for a saddle point field configuration,  $\Phi_{\sigma}$ , is the manifestation of the instanton gas [10]. Calculations are done on the  $6 \times 6$  lattice with  $N_t = 512$  and  $\beta = 20$ . The action is plotted with respect to the action of 3-instantons saddle point. (b) Number of instantons plus anti instantons corresponding to the maximum in the distribution of the instanton number (density of instantons) depending on the interaction strength. We compare the QMC results obtained on  $6 \times 6$  and  $12 \times 12$  lattices (note the rescaling of the  $12 \times 12$  lattice data to bring it to the same scale) with the prediction of the instanton gas model with hardcore repulsion between instantons.  $N_t$  and  $\beta$  are the same as for the plot (a).

gas formalism for the Hubbard model. Sec. III gives an account of the Monte Carlo process bounded within the designated set of thimbles. Here we equally demonstrate that this approximation yields surprisingly good results for spin and charge order parameters as well as for the single-particle spectral functions. Finally in Sec. IV we summarize our results and discuss further perspectives.

## II. LEFSCHETZ THIMBLES FORMALISM AND INSTANTON GAS APPROACH FOR THE HUBBARD MODEL

### II.1. Lefschetz thimbles formalism for the Hubbard model

The Hubbard model on a bipartite lattice can be written in particle-hole basis as:

$$\hat{H} = \hat{H}_{tb} + \hat{H}_\mu + \hat{H}_U = -\kappa \sum_{\langle \mathbf{x}, \mathbf{y} \rangle} (\hat{a}_\mathbf{x}^\dagger \hat{a}_\mathbf{y} + \hat{b}_\mathbf{x}^\dagger \hat{b}_\mathbf{y} + \text{h.c.}) + \mu \sum_{\mathbf{x}} q_{\mathbf{x}} + \frac{U}{2} \sum_{\mathbf{x}} \hat{q}_{\mathbf{x}}^2, \quad (2)$$

where  $\hat{a}_\mathbf{x}$  and  $\hat{b}_\mathbf{x}$  are annihilation operators for electrons and holes, and  $\hat{q}_\mathbf{x} = \hat{a}_\mathbf{x}^\dagger \hat{a}_\mathbf{x} - \hat{b}_\mathbf{x}^\dagger \hat{b}_\mathbf{x}$  is excess electrical charge at site  $\mathbf{x}$  with respect to the half-filling condition. The kinetic energy includes hoppings between sites belonging to different sublattices. In the following, all dimensional parameters including interaction strength  $U$  are expressed in units of the hopping  $\kappa$ . We included the chemical potential  $\mu$  to consider some general properties of the partition function and the thimble decomposition, however,  $\mu$  is set to zero in practical simulations.

We are interested in the path integral for the partition function

$$\mathcal{Z} = \text{Tr} \left( e^{-\beta \hat{H}} \right), \quad (3)$$

where  $\beta$  is the inverse temperature. After the introduction of the charge coupled continuous auxiliary field, the partition function can be written as follows [13, 14]:

$$\mathcal{Z} = \int \mathcal{D}\phi e^{-\int_0^\beta d\tau \sum_{\mathbf{x}} \frac{\phi_{\mathbf{x}}(\tau)^2}{2U}} \text{Tr} \left( e^{-\int_0^\beta d\tau \hat{H}(\hat{a}^\dagger, \hat{a}, \hat{b}^\dagger, \hat{b}, \phi(\tau))} \right),$$

$$\hat{H}(\hat{a}^\dagger, \hat{a}, \hat{b}^\dagger, \hat{b}, \phi(\tau)) = H_{tb} + H_\mu + i \sum_{\mathbf{x}} \phi_{\mathbf{x}}(\tau) \hat{q}_{\mathbf{x}}. \quad (4)$$

After Trotter decomposition and appropriate rescaling of the  $\phi$  field, we finally get

$$\mathcal{Z} = \int \mathcal{D}\phi e^{-S_B[\phi]} \det M_{el.}[\phi] \det M_{h.}[\phi],$$

$$S_B[\phi] = \sum_{\mathbf{x}, \tau} \frac{\phi_{\mathbf{x}, \tau}^2}{2U \Delta\tau}. \quad (5)$$

$\Delta\tau$  is the step in Euclidean time,  $N_\tau \Delta\tau = \beta$ . Auxiliary field  $\phi_{\mathbf{x}, \tau}$  is introduced for each site  $\mathbf{x}$  in each Euclidean time slice  $\tau$ .  $M_{el.}$  and  $M_{h.}$  are the fermionic operators for the electrons and holes respectively. The determinants of these operators are expressed as

$$\det M_{el.} = \det \left[ I + \prod_{\tau=1}^{N_\tau} D_{2\tau-1} D_{2\tau}^{el.} \right],$$

$$\det M_{h.} = \det \left[ I + \prod_{\tau=1}^{N_\tau} D_{2\tau-1} D_{2\tau}^{h.} \right], \quad (6)$$

where  $D_{2\tau}^{el.} \equiv \text{diag} \left( e^{i \text{Re} \phi_{\mathbf{x}, \tau} - \text{Im} \phi_{\mathbf{x}, \tau} + \mu \Delta\tau} \right)$ ,  $D_{2\tau}^{h.} \equiv \text{diag} \left( e^{-i \text{Re} \phi_{\mathbf{x}, \tau} + \text{Im} \phi_{\mathbf{x}, \tau} - \mu \Delta\tau} \right)$  and  $D_{2\tau+1} \equiv e^{-\Delta\tau h_{tb}}$  have been introduced (we included the possibility for the complexification of the fields  $\phi$ ). Both of these are  $N_S \times N_S$  matrices, where  $N_S$  is the total number of spatial lattice sites. We have also introduced  $h$ , which is the matrix characterizing the tight-binding part of the Hamiltonian  $\hat{H}$ . The determinant  $\det M_{el.}$  ( $\det M_{h.}$ ) is a result of the integration over the fermionic particle (hole) field  $\hat{a}$  ( $\hat{b}$ ).

The integral 5 can be rewritten in general form

$$\mathcal{Z} = \int \mathcal{D}\Phi e^{-S(\Phi)}, \quad (7)$$

where  $\Phi = \{\phi_{\mathbf{x}, \tau}\}$  is the set of all auxiliary fields, and the action includes both Gaussian part and logarithms of the fermionic determinants:

$$S = S_B(\Phi) - \ln \det M_{el.} - \ln \det M_{h.}. \quad (8)$$

The Lefschetz thimbles formalism [7] is a way to rewrite the general integral 7 using the information on the saddle points of the action  $S$ . The initial integral 7 is written for real auxiliary fields  $\Phi$ . However, the exponent  $e^{-S}$  in 7 is analytical function of the fields  $\Phi$ . Thus we can change the integration contour shifting it into complex plane without changing the final result for the partition function.

Let  $\Phi_\sigma$  be the saddle points of the action  $S$ . Note that the saddle points can be complex. Each saddle point features two manifolds emanating from it: the thimble,  $\mathcal{I}_\sigma$ , and the anti-thimble,  $\mathcal{K}_\sigma$ . Thimble  $\mathcal{I}_\sigma$  is a union of all solutions of the Gradient Flow (GF) equations

$$\frac{d\Phi}{dt} = \overline{\frac{\partial S}{\partial \Phi}}, \quad (9)$$

which start at the saddle point at flow time  $t = -\infty$ :  $\Phi(t) \in \mathcal{I}_\sigma$  if  $\Phi(t \rightarrow -\infty) \rightarrow \Phi_\sigma$ . The anti-thimble  $\mathcal{K}_\sigma$  consists of all possible solutions of the GF  $\Phi(t)$  which end up at a given saddle point  $\Phi_\sigma$ :  $\Phi(t) \in \mathcal{K}_\sigma$  if  $\Phi(t \rightarrow +\infty) \rightarrow \Phi_\sigma$ . We also need the number of intersections of an anti-thimble with real subspace:  $k_\sigma = \langle \mathcal{K}_\sigma, \mathbb{R}^N \rangle$ . Both thimble and anti-thimble are  $N$  dimensional real manifolds in complex space  $\mathbb{C}^N$ , where  $N = N_\tau N_S$  is the total number of auxiliary fields.

The important feature of the thimbles formalism is that by construction the imaginary part of the action is constant along the thimble. Assuming that we only sum over the relevant saddle points with  $k_\sigma = 1$ , we can write the final form of the partition function in the thimbles formalism as

$$\mathcal{Z} = \sum_{\sigma} e^{-i \text{Im} S(\Phi_\sigma)} \mathcal{Z}_\sigma, \quad (10)$$

$$\mathcal{Z}_\sigma = \int_{\mathcal{I}_\sigma} \mathcal{D}\Phi e^{-\text{Re} S(\Phi)}.$$

Particular saddle points can violate certain symmetries of the Hamiltonian. We would like to show that if one

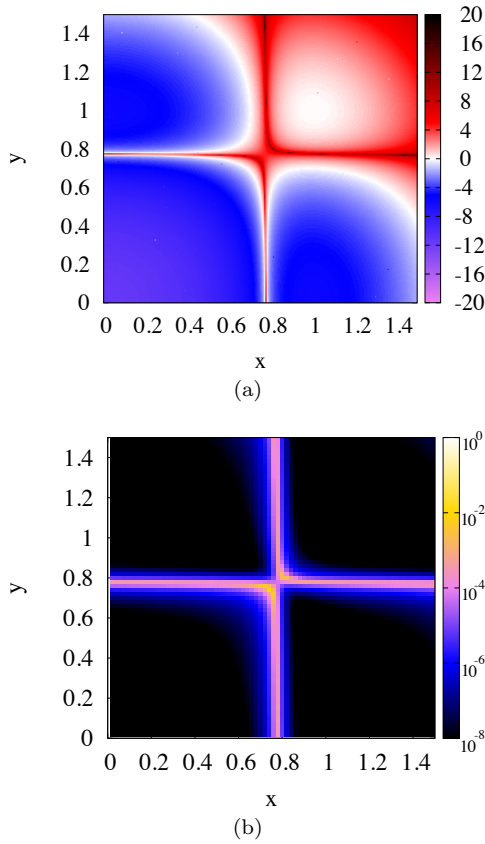


FIG. 2. (a) Action of the field  $\phi = x\phi^{(1)} + y\phi^{(2)}$  where  $\phi^{(i)}$  are single instanton configurations at different space time positions. Thus (1,1) point is two-instanton saddle, (0,1) and (1,0) are different one-instanton saddles and (0,0) is the vacuum. The distance between the two instantons is set to 3 lattice constants in real space and  $\delta\tau = 10$  in Euclidean time. The color scale is linear with zero corresponding to the action of the two-instanton saddle point. (b) The ratio of the long range spin-spin correlator to the short-range spin-spin correlator 18. Note the logarithmic color scale. Computations for both plots were carried out on a  $6 \times 6$  lattice at  $\beta = 20$  and interaction strength  $U = 6$ .

constrains integration over the set of thimbles that due to symmetry considerations share the very same saddle point value of the action then we obtain a symmetry consistent approximation. First of all, the SU(2) spin symmetry is automatically satisfied since our Hubbard Stratonovich transformation does not break it: each field configuration enjoys SU(2) spin symmetry. Thus spatial and Euclidean times translations, point group and time reversal symmetries remain. As we'll show later, all these symmetries are broken for a specific field configuration, however, our sampling over dominant thimbles restores them all. Spatial and Euclidean times translations, as well as point group symmetry are considered in the next section. Here we concentrate on the time reversal symmetry and consider not only half-filling, but also the case with finite chemical potential.

Time reversal symmetry operator  $\hat{T} = -i\sigma_2 K$  acts on

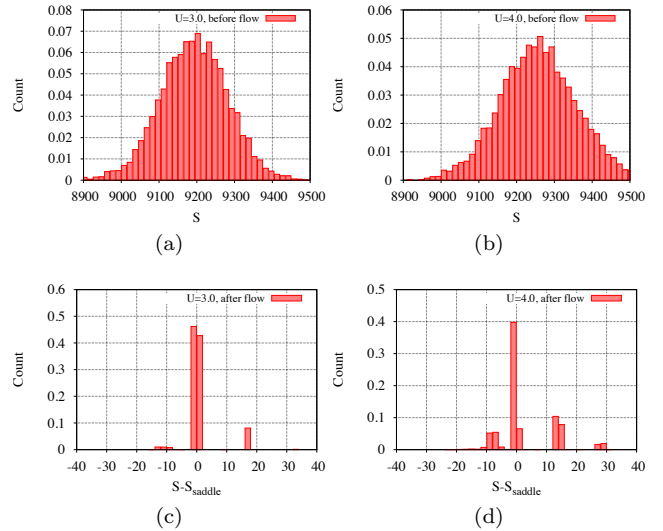


FIG. 3. (a) and (b) Histograms for the action of configurations proposed during the Monte Carlo process, before the downward GF. (c) and (d) Actions of the same configurations after downward GF. Calculations were made at  $6 \times 6$  lattice with  $\beta = 20$  and  $N_t = 256$ . Interactions strengths are  $U = 3.0$  (figures (a) and (c)) and  $U = 4.0$  (figures (b) and (d)).  $S_{saddle}$  is the action of the desired dominant saddle points.

spin indexes. Since the electrons and holes are connected with spin-up and spin-down electrons via the relation  $\hat{a}_{\mathbf{x}} = \hat{c}_{\mathbf{x},\uparrow}$ ,  $\hat{b}_{\mathbf{x}}^{\dagger} = \pm \hat{c}_{\mathbf{x},\downarrow}$  (the sign depends on sublattice), the charge can be written as  $\hat{q}_{\mathbf{x}} = \hat{c}_{\mathbf{x},\uparrow}^{\dagger} \hat{c}_{\mathbf{x},\uparrow} + \hat{c}_{\mathbf{x},\downarrow}^{\dagger} \hat{c}_{\mathbf{x},\downarrow} - 1$  and is not affected by the time reversal operator. In addition to that,  $\hat{T}$  includes complex conjugation of the  $\phi$  field. Consequently, we can write down the transformation of the Hamiltonian 4 as:

$$\hat{T}^{-1} \hat{H}(\hat{a}^{\dagger}, \hat{a}, \hat{b}^{\dagger}, \hat{b}, \phi(\tau)) \hat{T} = \overline{\hat{H}(\hat{a}^{\dagger}, \hat{a}, \hat{b}^{\dagger}, \hat{b}, \phi(\tau))} = \hat{H}(\hat{a}^{\dagger}, \hat{a}, \hat{b}^{\dagger}, \hat{b}, -\text{Re } \phi(\tau) + i \text{Im } \phi(\tau)). \quad (11)$$

Thus, after integrating out the fermionic fields in 5 we get action 8 where the following replacement of signs of  $\text{Re } \phi$  is made in fermionic operators:  $D_{2\tau}^{eL} \rightarrow \text{diag}(e^{-i \text{Re } \phi_{\mathbf{x},\tau} - \text{Im } \phi_{\mathbf{x},\tau} + \mu \Delta\tau})$ ,  $D_{2\tau}^{hL} \rightarrow \text{diag}(e^{i \text{Re } \phi_{\mathbf{x},\tau} + \text{Im } \phi_{\mathbf{x},\tau} - \mu \Delta\tau})$ . Thus the conservation of time reversal symmetry at the level of action is certain since the effective action 8 still respects the symmetry

$$S(-\text{Re } \Phi + i \text{Im } \Phi) = \overline{S(\text{Re } \Phi + i \text{Im } \Phi)}. \quad (12)$$

However, after the shift of the integration contour to the complex space, this symmetry is satisfied configuration-wise (and not after the full integration over all thimbles 10 is carried out) only if both configurations  $\Phi$  and  $-\Phi$  are included in the new integration contour, constructed using GF equations 9. Using the Cauchy-Riemann con-

ditions, the eq. 9 can be rewritten as

$$\begin{aligned} \frac{d \operatorname{Re} \Phi}{dt} &= \frac{\partial \operatorname{Re} S}{\partial \operatorname{Re} \Phi} \\ \frac{d \operatorname{Im} \Phi}{dt} &= \frac{\partial \operatorname{Re} S}{\partial \operatorname{Im} \Phi}. \end{aligned} \quad (13)$$

After the replacement  $\operatorname{Re} \Phi \rightarrow -\operatorname{Re} \Phi$ ,  $\operatorname{Im} \Phi \rightarrow \operatorname{Im} \Phi$  and taking into account the symmetry 12, we can conclude that  $\frac{d \operatorname{Re} \Phi}{dt}$  changes sign, but  $\frac{d \operatorname{Im} \Phi}{dt}$  remains the same. Thus for each thimble emanating from saddle point  $\Phi_\sigma$  we have its counterpart attached to saddle point  $-\Phi_\sigma$ , and using the relation  $\Phi \rightarrow -\Phi$ , we can switch between these two thimbles.

Thus in order to restore the time reversal symmetry, we should simply automatically take into account all symmetrical (with equal  $\operatorname{Re} S$  but opposite  $\operatorname{Im} S$ ) configurations, which differ only by the sign of  $\operatorname{Re} \Phi$ . This restoration of the time reversal symmetry will be employed in all subsequent simulations.

In general, the expression 10 does not lead to a smaller sign problem, despite the elimination of the fluctuations of the imaginary part of the action under the integral. The problem is that many thimbles with different  $\operatorname{Im} S$  can participate in the sum, such that cancellation effects can still be severe. A secondary effect is the fluctuation of the complex measure in the integral over the thimble since it is in general a curved manifold in complex space. It was shown [9, 12] that these fluctuations are not significant, at least for relatively small systems considered up to now.

It is impossible to predict the dominant thimble before performing simulations for a generic model. However, in the particular case of the Hubbard model with charge coupled auxiliary field, there is an approximation, which can predict the dominant thimbles quite precisely without any Monte Carlo input, relying solely on the parameters of the Hamiltonian 2 and inverse temperature  $\beta$ . This is the instanton gas approximation discussed in Ref. [10]. Since we know the dominant thimbles in advance we can constrain the Monte Carlo sampling to them thereby neglecting other thimbles in the sum 10. As we will show later, this approach completely eliminates the fluctuations of  $\operatorname{Im} S$ , thus it also frees us from the necessity to switch between thimbles separated by the domain walls formed by the zeros of fermionic determinants during the generation of the field configurations in the Monte Carlo process. This can substantially ease the ergodicity issues, which the formulations with continuous fields are prone to [13, 14].

In this paper we concentrate on the half-filling case and confront the results of simulations over the dominant thimbles to results of full QMC simulations. Since at half-filling all thimbles are confined within the real subspace, we are also free from difficulties originating from the need to generate the field configuration confined within the curved manifold in complex space. This greatly facilitates the computations, and provides an excellent proof of principle for the dominant thimbles ap-

proach.

Our tests were carried out for the Hubbard model on hexagonal lattice. It was shown in [10] that the instanton gas approximation is also fully valid for the square lattice Hubbard model. Thus we expect that the results of our calculations are also applicable to the square lattice.

## II.2. Instanton gas approximation and the role of zeros of the fermionic determinant

Figure 1(a) shows an example of the histogram demonstrating the relative importance of various saddle points for the Hubbard model. We start from the field configurations generated according to 7 in a normal Quantum Monte Carlo process using the Hybrid Monte Carlo algorithm [13–16]. Each configuration subsequently serves as a starting point for the inverse GF evolution (same as 9, but with negative sign on the right hand side). At half filling thimbles are confined within the real subspace, thus this flow ends in the local minimum of the action. In the complex plane, this local minimum is the saddle point, that defines the thimble, hence the initial configuration belongs to this thimble. The histogram of the action of these final saddle point field configurations shows the relative importance of different thimbles within the initial integral for the partition function 7.

As one can see, the distribution of the actions of saddle points is discrete, which corresponds to integer number of localized objects within each saddle point. These objects we identified as instantons and anti-instantons [10]. The only difference between them is the sign of  $\operatorname{Re} \Phi$  (with  $\operatorname{Im} \Phi = 0$  at half filling). The saddle point  $\Phi_\sigma$  is now defined through the number of instantons and anti-instantons ( $N_+$  and  $N_-$  respectively) and their coordinates in space  $\mathbf{X}$  and Euclidean time  $T$ :

$$\sigma = \{(\mathbf{X}_1, T_1) \dots (\mathbf{X}_{N_+}, T_{N_+}), (\mathbf{X}_{N_++1}, T_{N_++1}) \dots (\mathbf{X}_{N_++N_-}, T_{N_++N_-})\}. \quad (14)$$

Instantons are interacting only weakly [10], thus the actions of the saddle points can be approximated as

$$S_{N_+, N_-} = S_0 + N_+ S^{(1)} + N_- \bar{S}^{(1)}, \quad (15)$$

where  $N_+$  and  $N_-$  are number of instantons and anti-instantons respectively,  $S_0$  is action of vacuum saddle (corresponds to zero fields  $\Phi = 0$ ) and  $S^{(1)}$  is action of one instanton. Contributions of instanton and anti-instanton in the action are equal at half filling since the action is real  $\operatorname{Im} S^{(1)} = 0$ . Due to translational symmetry of the action and localized nature of (anti)instantons, their actions are also independent on their coordinates  $(\mathbf{X}_i, T_i)$ . Thus all distribution show us the total number of instantons and anti-instantons in the saddle point  $N_+ + N_-$ , and each peak in Fig. 1(a) is in fact a collection of equivalent saddles with fixed  $N_+ + N_-$  but different individual numbers of (anti)instantons and coordinates of these objects. The maximum of the distribution in



Fig. 1(a) gives us the instanton density in the dominant saddles. This density can be predicted even without plotting such histograms, using the model of instantons as a weakly interacting gas in 2+1D Euclidean volume [10]. Comparison of this prediction with real QMC results is shown in Fig. 1. As one can see, the prediction is reasonably accurate.

Unfortunately, this prediction is not enough to reproduce fully the physics of the Hubbard model. As was shown in [10], the pure saddle point approximation corresponds to increasingly localized, but disordered spins. In fact, with this saddle point approximation, it was not possible to reproduce the Gross-Neveu transition and appearance of the gap at the Dirac point, which for the Hubbard model on honeycomb lattice occurs at  $U \simeq 3.8$  [17].

Let us investigate more deeply the reasons behind this deficiency. Fig. 2(a) shows the profile of the action 8 along a two-dimensional cross-section of the configuration space defined as follows. Consider two field configurations  $\phi_{\mathbf{x},\tau}^{(1)}$  and  $\phi_{\mathbf{x},\tau}^{(2)}$  corresponding to single instantons at different locations. The point  $(x, y)$  in Fig. 2(a) corresponds to the field configuration  $\phi = x\phi^{(1)} + y\phi^{(2)}$  such that  $(0, 0)$  corresponds to the vacuum,  $(1, 1)$  to a two instanton saddle point and  $(1, 0)$  and  $(0, 1)$  to single instanton saddles. Due to the translational invariance, the action is the same at two latter saddles. One can clearly see the domain walls separating the saddles. They are formed by configurations, where the action goes to  $+\infty$ . These domain walls are nothing else but zeros of fermionic determinants. Naively, the weight of these configurations tends to zero within the integral for the partition function 5. However, their real role is enhanced by the fact that at least some observables diverge at these points. This phenomenon was studied in details in [18] where it was argued that these domain walls are responsible for the fat tails of the distributions of the fermionic observables. Here we only briefly repeat the reasoning behind this fact, while the interested reader can look into the paper [18] for mathematical details. The zeros of the fermionic determinant corresponds to the situation where the corresponding fermionic operator has a zero eigenvalue. Typical fermionic observable computed through the Wick theorem includes some combination of the inverse fermionic operators (fermionic propagators). Due the presence of zero eigenvalues, the latter diverge once we approach the domain walls between thimbles. In order to reveal the influence of the domain walls onto the long range spin order, we plot the ratio of long range spin-spin correlations to short range spin-spin correlations for the same 2D cross section in configuration space. Generally, the spin-spin correlator for sites within the same sublattice is computed as an average over configurations  $\Phi$ , generated with the weight 7:

$$\langle \hat{S}_{\mathbf{x}} \hat{S}_{\mathbf{x}+\mathbf{r}} \rangle = \lim_{N_{conf.} \rightarrow +\infty} \frac{1}{N_{conf.}} \sum_{\Phi} C_{\mathbf{x},\mathbf{x}+\mathbf{r}}(\Phi), \quad (16)$$

where  $N_{conf.}$  is the number of generated configurations

and

$$C_{\mathbf{x},\mathbf{x}+\mathbf{r}}(\Phi) = \frac{3}{4} (|g_{\mathbf{x},\mathbf{x}+\mathbf{r}}(\Phi)|^2 + |g_{\mathbf{x}+\mathbf{r},\mathbf{x}}(\Phi)|^2). \quad (17)$$

$g_{\mathbf{x},\mathbf{x}+\mathbf{r}}(\Phi)$  is the equal time fermionic propagator for electrons computed for the configuration of auxiliary fields  $\Phi$ . We plot the ratio of observables  $C_{\mathbf{x},\mathbf{x}+\mathbf{r}}(\Phi)$  for individual configurations

$$R(\Phi) = \frac{C_{\mathbf{x},\mathbf{x}+\mathbf{L}}(\Phi)}{C_{\mathbf{x},\mathbf{x}+\mathbf{r}_0}(\Phi)}. \quad (18)$$

Here  $\mathbf{L}$  corresponds to maximum spatial distance on the lattice and  $\mathbf{r}_0$  corresponds to the distance to the next-to-nearest neighbour lattice site.

The ratio  $R(\Phi)$  is plotted on Fig. 2(b). The ratio is negligibly small for the configurations near the saddle points, but quickly increases once we approach the domain walls formed by the zeros of the fermionic determinants. Now the deficiency of the saddle point approximation is evident: in fact, for the particular case of the charge coupled auxiliary fields the configurations away of the saddle points are responsible for the long range spin order.

Many question now arises. What is the quality of the approximation in which we constrain the Monte Carlo sampling to the dominant thimbles? As opposed to the instanton gas approximation, can it account for symmetry breaking mass generation?

### III. QMC ON A LIMITED SET OF THIMBLES

Our aim is to construct a Monte Carlo algorithm, which will generate the auxiliary field configurations according to the distribution  $e^{-S(\Phi)}$  in the restricted space of thimbles,  $\mathcal{I}_{\sigma}, \sigma \in D$  attached to dominant saddle points. The corresponding partition function is written as:

$$\mathcal{Z}_D = \sum_{\sigma \in D} \int_{\mathcal{I}_{\sigma}} D\Phi e^{-S(\Phi)}. \quad (19)$$

In order to restrict the Monte Carlo process within the designated thimbles, we modify the generation of auxiliary field configurations. First, the proposal of the new configuration is made in the same manner as it is done in the Hybrid Monte Carlo (HMC) technique: via artificial Hamiltonian dynamics for potential equal to the action 8 [13, 15, 16]. Ideal Hamiltonian dynamics cannot cross the domain wall of infinite potential. However, an instanton-anti-instanton pair can be created without crossing the domain wall [10]. In addition to this effect, the numerical Hamiltonian dynamics can occasionally cross the domain wall due to the finite MD time step. Thus the usual Metropolis accept-reject step from HMC algorithm should be supplemented by an additional check that the proposed new configuration still belongs to the designated thimble. This check is done in the same

manner as the construction of the histogram 1(a). We perform the inverse GF according to the equation 9 with minus sign on the right hand side and starting from the proposed configuration. This gradient flow ends up in the saddle point for the thimble, which the proposed configuration belongs to. We check that this saddle point at the end of the flow has still the same number of instantons and anti-instantons as the desired saddle, and accept the proposed configuration only if this is true. An illustration of this process is shown in the figure 3 for two simulations for  $U = 3.0$  and  $U = 4.0$ . We plot histograms of the actions of the proposed configuration alongside with the histograms of the actions of the configurations after the downward GF. The former histograms show broad and featureless distributions, while the latter show discrete distributions similar to fig. 1(a). It gives us a quite simple criterion for the additional accept/reject step of the Monte Carlo algorithm: only those proposed configurations can be accepted, where the action after the inverse GF falls in the peak corresponding to the desired saddle.

In practice we start from the single dominant saddle point field configuration predicted by the instanton gas model, which gives us the number of instantons  $N_+$  and anti-instantons  $N_-$  and their coordinates  $(X_i, T_i)$ .  $N_+ = N_-$ , since the most probable configuration must have equal number of instantons and anti-instantons for obvious combinatorial reasons [10]. After the MC update and downwards GF we only check that we returned back to the saddle with the same action and  $N_+ = N_-$  as the starting field configuration. Since we do not control the coordinates of individual (anti)instantons, they are allowed to move freely through the lattice. HMC can facilitate this move, since it is possible to change the spatial location of the instanton by tunneling through the local peak of the action. One can observe that it is possible to construct a trajectory connecting points  $(1, 0)$  and  $(0, 1)$  in Fig. 2(a) without crossing the domain wall of zeros of determinant. Since these points on the figure correspond to the instantons at different spatial locations, free movement between such points restores spatial translational and rotational symmetries. Movement along the Euclidean time axis is even simpler since it corresponds to the continuous symmetry (in the limit  $\Delta\tau = 0$ ), thus

there should be no domain walls between field configurations  $\{\phi_{x,\tau}\}$  and  $\{\tilde{\phi}_{x,\tau}\} = \{\phi_{x,\tau+1}\}$ , at least if  $\Delta\tau$  is small enough. In the saddle point approximation, this movement corresponds to the zero mode of Hessian of the saddle point, discussed extensively in [10].

Algorithm constructed in this way stays indefinitely within the series of interconnected thimbles with fixed  $N_+$  and  $N_-$  numbers. These thimbles are attached to the dominant saddle points, thus giving us the desired approximation to the integral for the partition function 19, where  $D$  is a set of all possible saddle points with fixed  $N_+$  and  $N_-$ , but different coordinates of individual (anti)instantons. We stress that despite formally multiple thimbles participate in the partition function, the fluctuations of  $\text{Im } S$  would still be absent even away of half filling, since the  $\text{Im } S$  is fully defined by  $N_+$  and  $N_-$  numbers 15.

Configurations generated with this algorithm are subsequently used for the calculation of the fermionic observables. First we look at charge and spin order parameters. Following [14] we compute squared spin per sublattice

$$\langle \hat{S}^2 \rangle = \left\langle \left( \sum_{\mathbf{x} \in A} \hat{S}_{\mathbf{x}} \right)^2 \right\rangle \quad (20)$$

and squared charge per sublattice

$$\langle \hat{Q}^2 \rangle = \left\langle \left( \sum_{\mathbf{x} \in A} \hat{q}_{\mathbf{x}} \right)^2 \right\rangle, \quad (21)$$

where  $A$  denotes one of the two sublattices of the bipartite lattice. These observables can be rewritten in terms of averages over configurations of auxiliary fields generated according to the distributions in 7 or 19:

$$\langle \hat{S}^2 \rangle = \lim_{N_{conf.} \rightarrow +\infty} \frac{3}{4N_{conf.}} \sum_{\Phi} \left( \sum_{\mathbf{x}, \mathbf{y} \in A, \mathbf{x} \neq \mathbf{y}} C_{\mathbf{x}, \mathbf{y}}(\Phi) + \sum_{\mathbf{x} \in A} (1 - 2 \text{Re } g_{\mathbf{x}, \mathbf{x}}(\Phi) + 2|g_{\mathbf{y}, \mathbf{x}}(\Phi)|^2) \right) \quad (22)$$

$$\langle \hat{Q}^2 \rangle = \lim_{N_{conf.} \rightarrow +\infty} \frac{2}{N_{conf.}} \sum_{\Phi} \left( \sum_{\mathbf{x} \in A} (\text{Re } g_{\mathbf{x}, \mathbf{x}}(\Phi) - |g_{\mathbf{x}, \mathbf{y}}(\Phi)|^2) + \sum_{\mathbf{x}, \mathbf{y} \in A, \mathbf{x} \neq \mathbf{y}} \text{Re} (g_{\mathbf{x}, \mathbf{x}}(\Phi)g_{\mathbf{y}, \mathbf{y}}(\Phi) - g_{\mathbf{x}, \mathbf{y}}(\Phi)g_{\mathbf{y}, \mathbf{x}}(\Phi) - g_{\mathbf{x}, \mathbf{x}}(\Phi)g_{\mathbf{y}, \mathbf{y}}^*(\Phi)) \right) \quad (23)$$

Real parts of the expression are taken in order to account for trivial symmetry of the action 8 with respect to the exchange of the sign of real part of the  $\Phi$  field. It

means that for each configuration, there is a counterpart with exactly the same weight in the partition function but opposite real parts of the fields, which corresponds

to the exchange of  $g$  and  $\bar{g}$  in all fermionic observables. According to the discussion concerning the time reversal symmetry in the section II.1, it corresponds to the enhanced estimator restoring the time-reversal symmetry.

For the benchmark QMC calculation, we use field configurations  $\Phi$  generated according to the distribution in 7, whereas for the dominant thimbles approximation, the distribution of 19 is sampled. The complete simulation spanning over all thimbles can be done via the addition of the small second auxiliary field coupled to spin density. It helps the Hybrid Monte Carlo to penetrate through the domain walls by increasing the overall dimensionality of the configuration space [13, 14].

Benchmarks are shown in Figs. 4(a) and 4(b). In addition to the dominant thimbles results, we also show the results of the simulation over the thimble attached to the wrong saddle point: many instanton saddle at small  $U$  and vacuum at large  $U$ . The squared spin results are rescaled using critical exponents corresponding to the first order  $\epsilon$ -expansion,  $\beta/\nu = 0.9$  (see Ref. [19] for the accuracy of this approximation). With this rescaling the critical point corresponds to the coupling constant at which the scaled square spin is independent on the system size.<sup>1</sup>

As one can see, the dominant thimbles results are hardly distinguishable from the full simulation for both  $6 \times 6$  and  $12 \times 12$  lattices. This implies that we have similar crossing points for the full and dominant thimbles approximation. In Fig. 4(b) we see that the squared charge does not decay with increased interaction strength if we are using wrong saddle point. This is in line with the previously reported results of [14], where the results for squared charge were reported to deviate from the correct ones due to the ergodicity issues with the single field HMC algorithm: in this case MD can not cross the domain walls between different thimbles.

As a final check, we compute the single electron spectral function in the dominant thimbles simulation. We compute it using Euclidean time fermionic propagator and the Algorithms for Lattice Fermions (ALF) [20] implementation of the Stochastic analytical continuation [21, 22] to real time. The saddle point approximation [10] leads to the absence of the mass gap at the Dirac point even in the strong coupling limit. On the contrary, in the dominant thimbles approximation, the spectral function is hardly distinguishable from the one obtained in the full simulation. Thus we can conclude that it is indeed enough to only simulate the limited set of dominant thimbles in order to obtain the Mott insulator with long range Antiferromagnetic (AFM) spin order at  $U > 4$ .

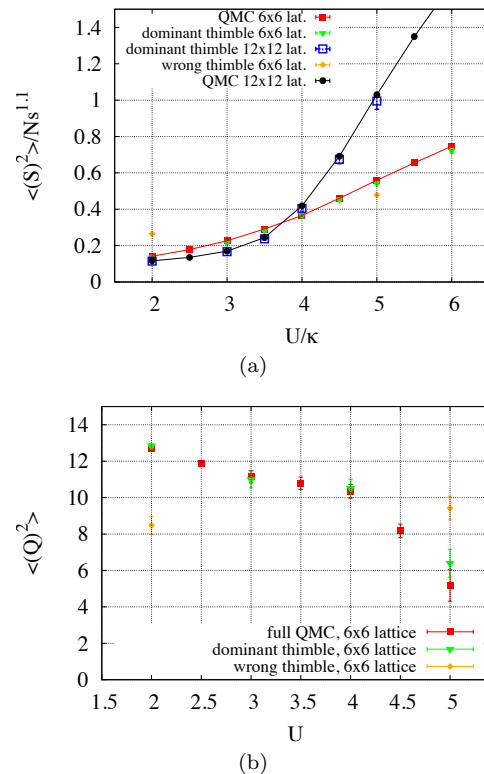


FIG. 4. Squared spin (a) and squared charge (b) on sublattice computed using full QMC 7 and with Monte Carlo process constrained to a single thimble 19. Rescaling is done for the squared spin observable using critical exponents of the first order  $\epsilon$ -expansion,  $\frac{\langle S^2 \rangle}{N_s^2} = N_s^{-\beta/\nu} F(L^{1/\nu}(U - U_c))$ . Here we omit correction to scaling. The dominant saddle points are always predicted using instanton gas model with hardcore repulsion. The *wrong thimble* results at  $U = 2.0$  refer to the one attached to the 40-instanton saddle on a  $6 \times 6$  lattice (the true dominant saddle is the vacuum one in this case); wrong thimble at  $U = 5.0$  means the one attached to vacuum, while true dominant saddles contain 25 (anti)instantons. Calculations were done on  $6 \times 6$  and  $12 \times 12$  lattices with  $\beta = 20$  and  $N_t = 256$ .

#### IV. CONCLUSION

We demonstrated that the dominant thimbles approximation produces precise results for the Hubbard model at half-filling. In fact, within our precision the dominant thimbles results match precisely with our benchmark results. In particular, we showed the appearance of long range spin-spin order with concomitant suppression of the squared charge. Additionally, the single particle spectral function shows the appearance of the gap in the spectrum at the Dirac point and the imaginary time Green functions of the dominant thimbles approximation turns out to be very close to our benchmark result.

The crucial feature of the considered dominant thimbles approximation is a understanding of the saddle point structure of the path integral. In our specific half-filled

<sup>1</sup> We omit corrections to scaling.



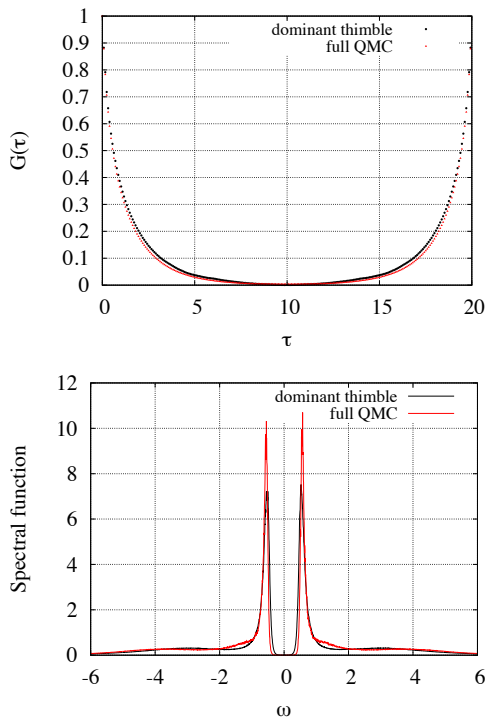


FIG. 5. Single-particle Euclidean time propagators (a) and corresponding spectral functions (b) at the Dirac point obtained in full QMC calculation and in the Monte Carlo process bounded within one dominant thimbles. Calculation was done on  $12 \times 12$  lattice for  $U = 5.0$  at inverse temperature  $\beta = 20$ .

particle-hole symmetry case, this knowledge stems from the instanton gas approximation discussed in [10]. This insight provides a classification of saddle points in terms of instantons and anti-instantons, and it is possible to predict the number of instantons and anti-instantons in the dominant saddle points. This information suffices to constrain the simulation to a series of dominant thimbles. The half-filled case turns out to be especially simple since thimbles are constrained to the real space. Generically, the thimble is curved manifold in complex space, and it is considerably more complicated to construct it.

As we showed above, the dominant thimbles approximation does not break any symmetries of the Hamiltonian. Furthermore, we observe a transition to an antiferromagnetic insulating state, that certainly seems to be continuous given our admittedly limited data set. Since generically symmetries and dimensionality pin down uni-

versality, we conjecture that the quantum phase transition we observe within the dominant thimbles approximation belongs to the  $O(3)$  Gross-Neveu phase transition [23] as observed in the Hubbard model on the honeycomb lattice [19, 24, 25].

The most important consequence of our results, is a strong motivation to consider similar dominant thimble approximations also away of half filling. It was shown that the instanton gas approximation retains essentially the same structure also at finite chemical potential [26]. Thus the only modification required to implement this approach away from half-filling would be to construct (approximate) thimbles in complex space. While this is still a formidable task, we will be at least freed from the ergodicity issues connected with the necessity for the algorithm to jump between relevant thimbles with different values of  $\text{Im} S$ . This is sometimes difficult and need additional care [26, 27]. The only input for such an algorithm would be the *ab initio* prediction of the dominant thimbles for the case of non zero chemical potential from the complexified instanton gas approximation, which will be the subject of follow up papers.

We again stress that even away from half-filling, the dominant thimbles approximation does not explicitly break symmetries. At half-filling the approximation has the potential of accounting for long ranged order and concomitant spontaneous symmetry breaking. Away from half-filling we will not suffer for the sign problem such that irrespective on the the quality of the approximation our simulations will provide a *symmetry* consistent point of view on doping an antiferromagnetic Mott insulator.

## ACKNOWLEDGMENTS

MU thanks the DFG for financial support under the projects UL444/2-1. FFA acknowledges financial support from the DFG through the Würzburg-Dresden Cluster of Excellence on Complexity and Topology in Quantum Matter - *ct.qmat* (EXC 2147, Project No. 390858490) as well as the SFB 1170 on Topological and Correlated Electronics at Surfaces and Interfaces (Project No. 258499086). Computational resources were provided by the Gauss Centre for Supercomputing e.V. ([www.gauss-centre.eu](http://www.gauss-centre.eu)) through the John von Neumann Institute for Computing (NIC) on the GCS Supercomputer JUWELS [28] at Jülich Supercomputing Centre (JSC).

- 
- [1] M. Troyer and U.-J. Wiese, *Phys. Rev. Lett.* **94**, 170201 (2005), [arXiv:cond-mat/0408370](https://arxiv.org/abs/cond-mat/0408370) [cond-mat].
- [2] D. Hangleiter, I. Roth, D. Nagaj, and J. Eisert, *Science Advances* **6** (2020), [10.1126/sciadv.abb8341](https://advances.sciencemag.org/content/6/33/eabb8341), <https://advances.sciencemag.org/content/6/33/eabb8341.full.pdf>.
- [3] Z.-Q. Wan, S.-X. Zhang, and H. Yao, *Phys. Rev. B* **106**, L241109 (2022).
- [4] T. Sato and F. F. Assaad, *Phys. Rev. B* **104**, L081106 (2021).
- [5] E. W. Huang, R. Sheppard, B. Moritz, and T. P. Devereaux, *Science* **366**, 987 (2019), <https://www.science.org/doi/pdf/10.1126/science.aau7063>.

- [6] E. Witten, *AMS/IP Stud. Adv. Math.* **50**, 347 (2011), [arXiv:1001.2933 \[hep-th\]](#).
- [7] E. Witten, (2010), [arXiv:1009.6032 \[hep-th\]](#).
- [8] M. Cristoforetti, F. Di Renzo, and L. Scorzato (AuroraScience), *Phys. Rev.* **D86**, 074506 (2012), [arXiv:1205.3996 \[hep-lat\]](#).
- [9] M. Ulybyshev, C. Winterowd, and S. Zafeiropoulos, *Phys. Rev. D* **101**, 014508 (2020).
- [10] M. Ulybyshev, C. Winterowd, F. Assaad, and S. Zafeiropoulos, *Phys. Rev. B* **107**, 045143 (2023).
- [11] M. Abhishek and M. Cristoforetti, (2014), [arXiv:1403.5680 \[hep-th\]](#).
- [12] A. Alexandru, G. Basar, P. F. Bedaque, G. W. Ridgway, and N. C. Warrington, *Phys. Rev.* **D95**, 014502 (2017), [arXiv:1609.01730 \[hep-lat\]](#).
- [13] S. Beyl, F. Goth, and F. Assaad, *Phys. Rev.* **B97**, 085144 (2018), [arXiv:1708.03661 \[cond-mat.str-el\]](#).
- [14] P. Buividovich, D. Smith, M. Ulybyshev, and L. von Smekal, *Phys. Rev.* **B98**, 235129 (2018), [arXiv:1807.07025 \[cond-mat.str-el\]](#).
- [15] S. Duane, A. D. Kennedy, B. J. Pendleton, and D. Roweth, *Phys. Lett.* **B195**, 216 (1987).
- [16] R. T. Scalettar, D. J. Scalapino, R. L. Sugar, and D. Toussaint, *Phys. Rev. B* **36**, 8632 (1987).
- [17] F. F. Assaad and I. F. Herbut, *Phys. Rev. X* **3**, 031010 (2013).
- [18] M. Ulybyshev and F. Assaad, *Phys. Rev. E* **106**, 025318 (2022).
- [19] F. F. Assaad and I. F. Herbut, *Phys. Rev. X* **3**, 031010 (2013).
- [20] F. F. Assaad, M. Bercx, F. Goth, A. Götz, J. S. Hofmann, E. Huffman, Z. Liu, F. P. Toldin, J. S. E. Portela, and J. Schwab, *SciPost Phys. Codebases*, 1 (2022).
- [21] K. S. D. Beach, *arXiv e-prints*, cond-mat/0403055 (2004), [arXiv:cond-mat/0403055 \[cond-mat.str-el\]](#).
- [22] A. Sandvik, *Phys. Rev. B* **57**, 10287 (1998).
- [23] I. F. Herbut, V. Juričić, and B. Roy, *Phys. Rev. B* **79**, 085116 (2009).
- [24] F. Parisen Toldin, M. Hohenadler, F. F. Assaad, and I. F. Herbut, *Phys. Rev. B* **91**, 165108 (2015).
- [25] Y. Otsuka, S. Yunoki, and S. Sorella, *Phys. Rev. X* **6**, 011029 (2016).
- [26] M. Ulybyshev, C. Winterowd, and S. Zafeiropoulos, (2019), [arXiv:1906.07678 \[cond-mat.str-el\]](#).
- [27] M. Fukuma, N. Matsumoto, and N. Umeda, *Phys. Rev. D* **100**, 114510 (2019).
- [28] Jülich Supercomputing Centre, *Journal of large-scale research facilities* **5** (2019), 10.17815/jlsrf-5-171.